CHAPTER 10

EFFECT OF PRESSURE ON ELECTRICAL RESISTIVITY AND THERMOELECTRIC POWER OF WS_2

10.1 INTRODUCTION

Dichalcogenides of interest as self lubricating solids include the disulphides, diselenides and tellurides of the metals molybdenum, tungsten, niobium and tantalum. Whereas MoS_2 occurs naturally, the other chalcogenides are produced synthetically by direct combination of the elements at elevated temperature. They are relatively expensive and specialised materials and can be considered as direct substitute for MoS_2 where MoS_2 is limited by its relatively poor oxidation resistance above 400°C or by its relatively

high electrical resistivity.

A comparison between the physical properties of MoS_2 and WS_2 (Table 10.1) [1] suggests that WS_2 is isostructural with MoS_2 and has a relatively low electrical resistivity. It provides significantly better oxidation resistance during heating in air than MoS_2.

Tungsten disulphide has an advantage of about 100°C over MoS_2 with respect to oxidation resistance [1] and thermal stability. The relatively slow rates of oxidation of WS_2 were thought to be due to the formation of tungsten trioxide, WO_3, which is somewhat more protective against further oxidation and provides a lower coefficient of friction than molybdenum trioxide MoO_3.

The electrical resistivity values quoted in above Table 10.1 indicates that WS_2 can provide better high temperature, high pressure and electrical conduction than MoS_2. This property together with a low coefficient of friction, makes WS_2 appear promising for use in sliding electrical contacts. At present, sliding electrical contacts are being made with MoS_2 which has a much higher resistivity as compared to WS_2.

It is therefore worthwhile to study the effect

Table 10.1 Comparison between the physical properties of MoS_2 and WS_2

Property	MoS_2	WS_2
Molecular weight	160.08	248.05
Crystal structure	Hex.	Hex.
Lattice constants (A°)		
a	3.16	3.29
c	12.29	12.97
Volume resistivity*		
Ω in	336	5.7
Ω cm	851	14.4

*Measurements made on 1 x 0.250 x 0.125-in. bar hot-pressed at 200°C and 30,000 psi; measurements were made perpendicular to the pressing direction. Comparative volume resistivity of graphite is 0.00104 Ω in., or 0.00264 Ω cm.

of pressure on the physical properties of WS_2 synthesised using different techniques.

To the best of the knowledge of the author no high pressure studies have been reported on WS_2. A brief review of the work done on its isostructural compound MoS_2 is presented below :

Bridgman reported the appearance of a high pressure polymorph in MoS_2 at about 20 Kbar at room temperature [2]. The transformation was indicated by a discontinuous drop of 36 % in electrical resistance which was found to be reversible on decompression. Minomura and Drickamer [3] made room temperature resistance measurements over the range 30-480 Kbar, finding only a continuous drop in resistance with increasing pressure [3]. Connell, Wilson and Yoffe [4] studied the absorption spectrum at pressures up to 60 Kbar at both room and liquid nitrogen temperatures. No discontinuities were noted in the observed properties other than the disappearance of the second order exciton at about 5 Kbar. This exciton did not reappear upon decompression, and its loss was tentatively attributed to changes in the dislocation density during initial pressurization [4]. Grant et al.[5] studied the exciton spectrum of MoS_2 in a hydrostatic device to a maximum pressure of 6 Kbar and over a temperature range of 80-295 K

[5]. The linear compressibilities at 12 Kbar were determined by Flack from X-ray measurements with a diamond anvil cell containing a NaCl pressure calibrant [6]. Webbe et al. [7] carried out high pressure investigations of MoS_2 upto the pressures of 50 Kbar at ambient temperature. The measured electrical resistance upto 50 Kbar and the effect of pressure on the energy gap was found to agree with the previous work. Their compressibility data agreed well with the theoretical values derived from a model which assumed bond-stretching forces only. None of their experiments showed an evidence of phase transformation at nearly 20 Kbar as reported by Bridgman.

The present chapter describes the variation in resistance and thermoelectric power with pressure and temperature on single crystals of WS_2 grown with and without a transporting agent.

10.2 EXPERIMENTAL PROCEDURE

Sample Preparation

As grown single crystals of WS_2 grown with and without the help of a transporting agent (Chapter VIII) were classified into the following groups :

Crystal grown by Direct Vapour Transport (DVT) method :

1. Specimens having spirals on their grown faces.

2. Specimens having growth layers.
3. Specimens with absolutely plane faces

Crystal grown by Chemical Vapour Transport (CVT) (Iodine) method :

1. Specimens showing spirals
2. Specimens showing growth layers
3. Specimens with absolutely plane faces

High Pressure Measurements

A tungsten carbide opposed anvil set-up [8] with pyrophyllite gasket and talc or silver chloride pressure transmitting medium can be conveniently used for high pressure studies upto 100 Kbar. A resistivity cell used with this set-up for the resistance measurements of the samples under pressure is shown in Fig. 10.1.

The variation of the resistance of zone-refined 99.999 % pure bismuth with pressure is shown in Fig. 10.2. The pressure corresponding to the load at the minimum in the resistivity curve in Bi II phase was assigned the value 26.2 Kbar, which is the average of Bi I-II and Bi II-III transition pressures [9]. Similarly, the pressure corresponding to the load at the mid-point of Bi III-V transition was taken to be 76.7 Kbar [10]. A smooth curve

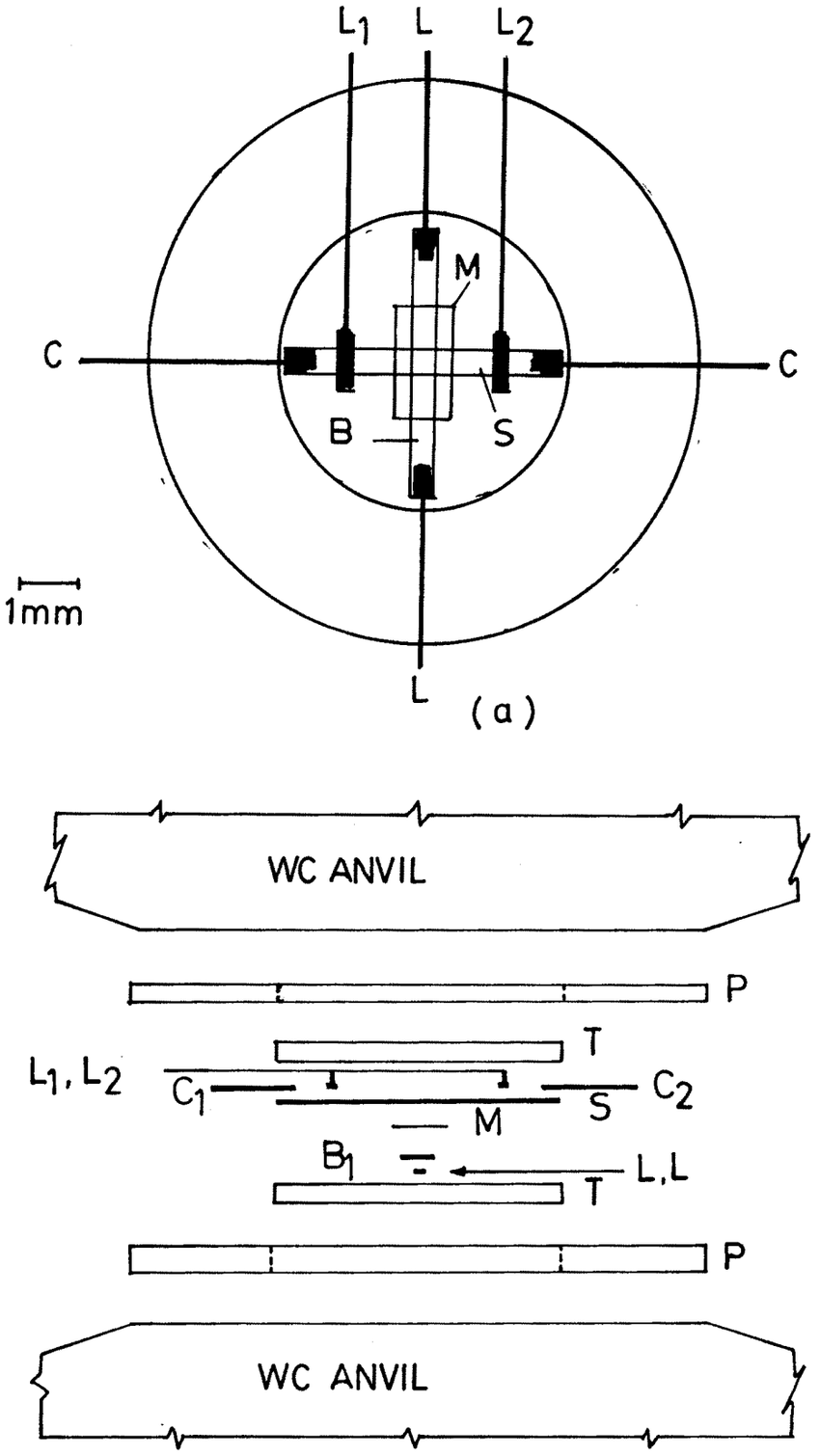

Resistivity cell for the opposed anvil set up
S specimen; C_1, C_2 current leads, L_1L_2 voltage leads; M, mica;
L, L, leads for bismuth pressure marker; P, pyrophyllite
gaskets; T, talc discs.

fig. 10·1

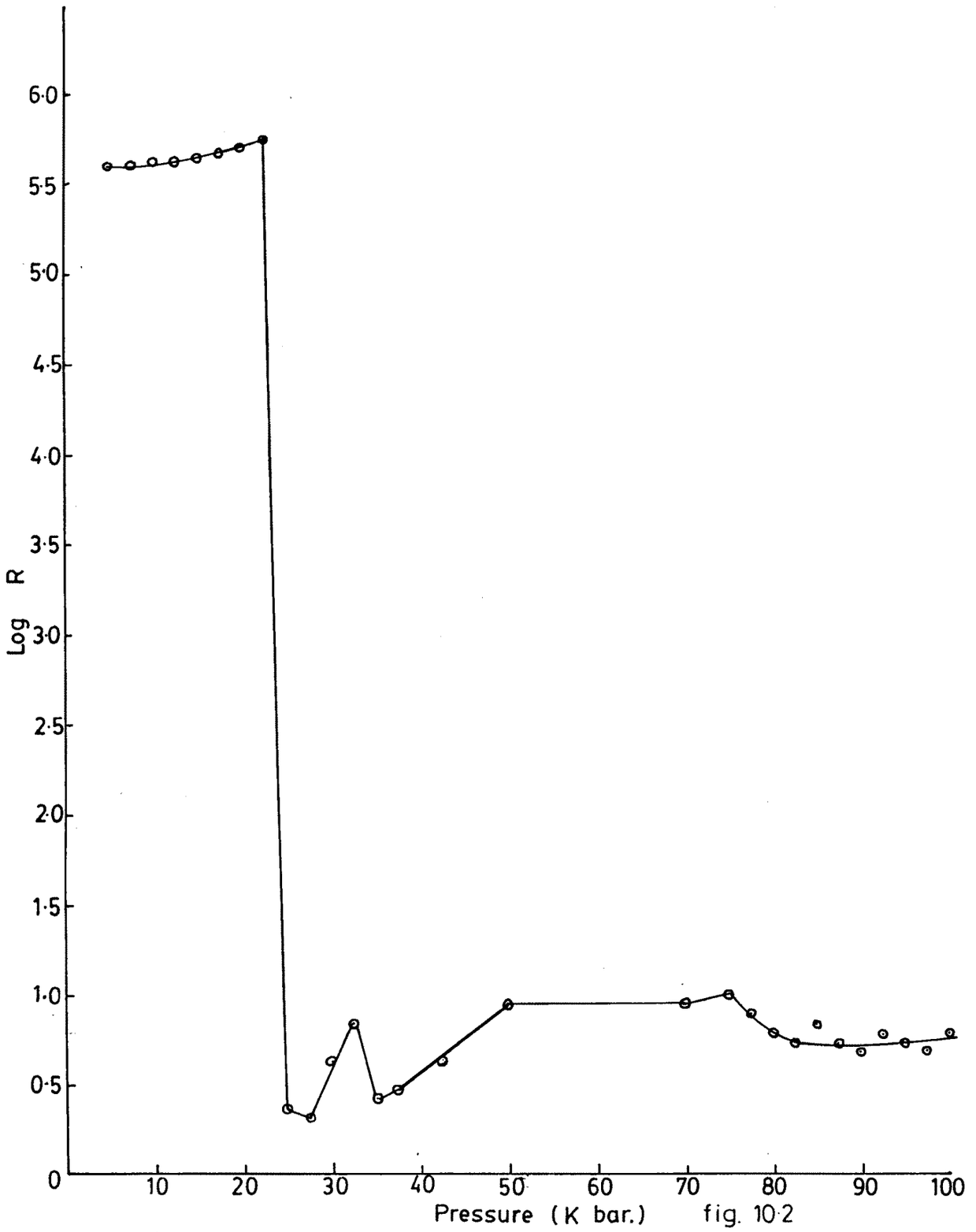
6·0
5·5
5·0
4·5
4·0
3·5
3·0
2·5
2·0
1·5
1·0
0·5
0
Log R
10
20
30
40
50
60
70
80
90
100
Pressure (K bar.)

fig. 10·2

through the origin and these fixed pressure points provided calibration to 80 Kbar.

The samples for resistance measurement were contained in the pyrophyllite gasket with talc as the pressure transmitting medium. A two probe technique was used to evaluate the resistance of the crystals. The resistance was measured on many independent runs on all the samples of WS_2 as a function of pressure and was found to be reproducible.

A cell [11] for the measurement of the thermoelectric power, S, is shown in Fig. 10.3. Simultaneous thermoelectric power S and resistance measurements to about 80 Kbar were conducted in 12.7 mm anvils. Details of the high pressure cell modelled after the design of Singh and Ramani [11] are as shown in Fig. 10.4 [12].

A temperature gradient was provided across the specimen by a nichrome wire heater connected to a 0-10 V constant voltage DC power supply, and the potentials E_N and E_M across the pairs of the chromel and alumel wires C_1C_2 and A_1A_2 were measured with a Keithley nanovoltmeter. The chromel and alumel wires were spot welded, and carefully held parallel to one another and normal to the sample length

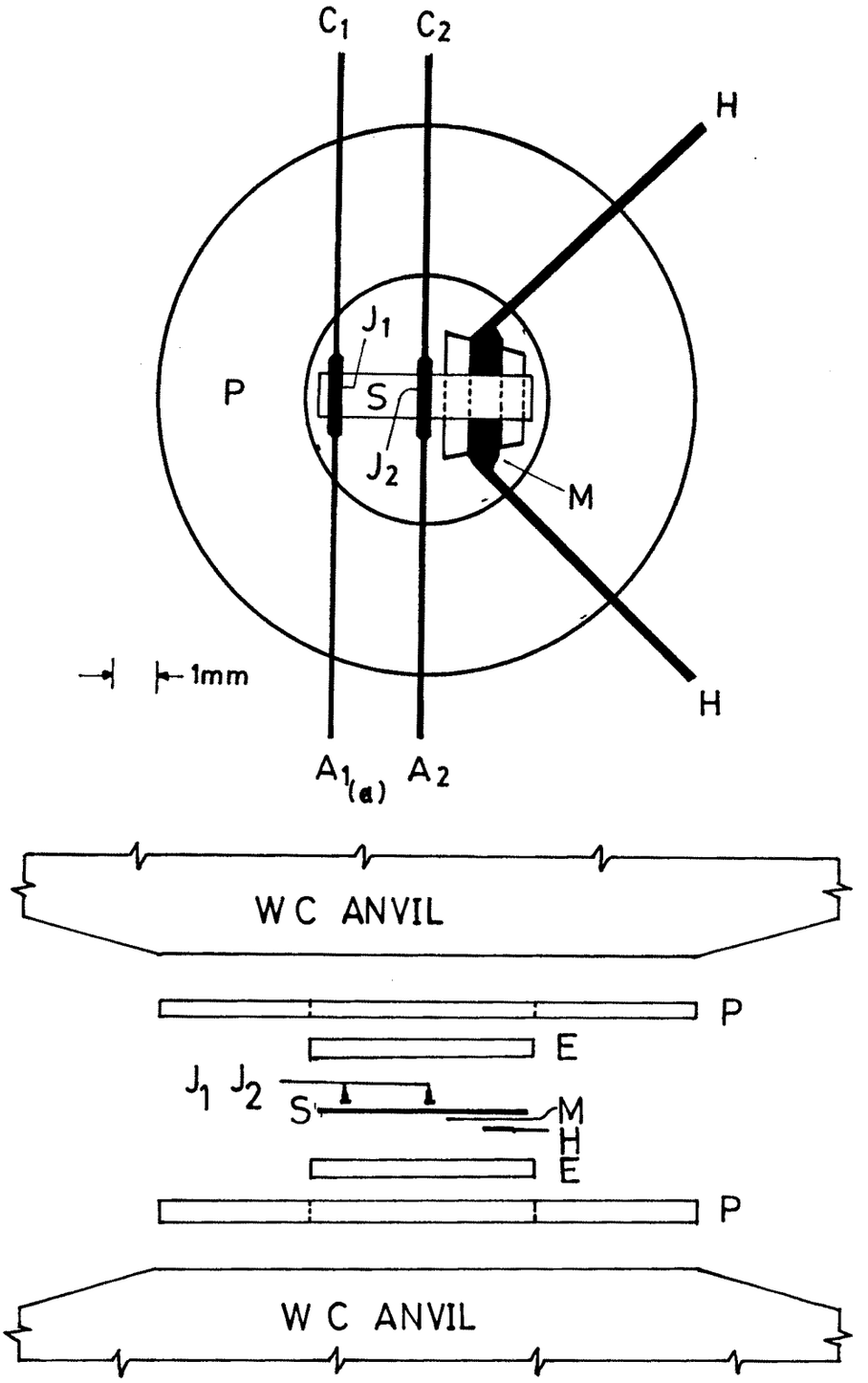

High pressure cell for the measurement of TEP using tungsten carbide opposed anvil set up [(a) View normal to the anvil face and (b) view parallel to the anvil face. P, pyrophyllite gasket E, epoxy or talc pressure transmitting disc S, specimen Heater M, mica insulation C_1 C_2 chromel A_1 A_2 alumel J_1 J_2 themrmojunctions]

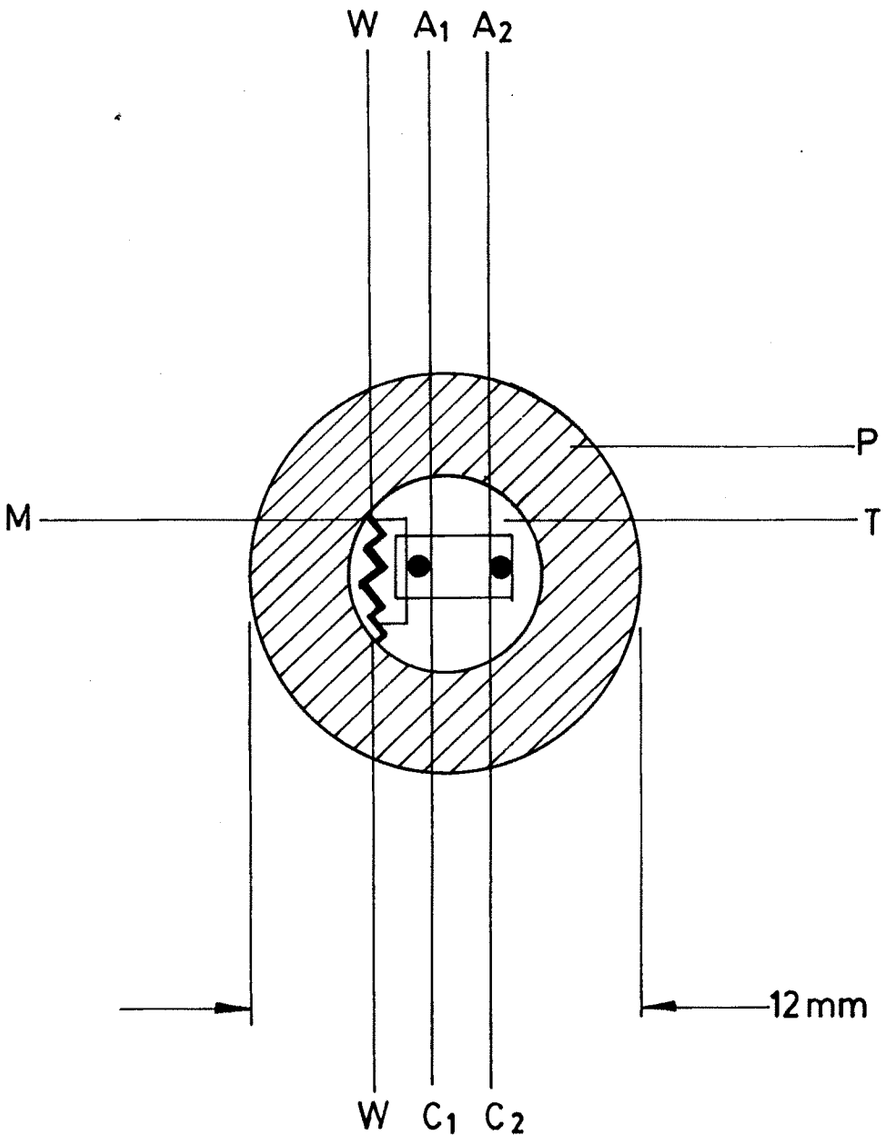

Sample assembly for Seebeck coefficient and resistivity measurements. P: pyrophyllite rings 12·50 o.d.x 5·3 mm i.d. and 0·3 mm (lower) 0·2 mm. (upper) thickness T: steatite disks; C_1 C_2, A_1 A_2: Chromel and Alumel wires 0·05 mm dia; W: Nichrome wire heater 0·03 mm dia; M: mica sheet. For the sake of clarity upper talc disk is not shown.

fig. 10·4

with their junctions pointing radially outwards so that the same temperature difference was maintained across the leads C_1C_2 and A_1A_2.

The thermoelectric power S of the specimen was evaluated from the measured values of E_N and E_M from the relationship [11].

$$Q = \frac{Q_A - \gamma Q_C}{1 - \gamma} \qquad (10.1)$$

where Q_C and Q_A are the thermoelectric powers of Chromel and Alumel respectively.

and $$\gamma = \frac{E_{AA}}{E_{CC}} = \frac{E_M}{E_N} \qquad [10.2]$$

The physical properties of Chromel and Alumel used in the evaluation of TEP are shown in Table 10.2

With values of Q for Alumel and Chromel substituted in the expression for TEP, we get

$$Q = - \frac{18.3 - 21.6\gamma}{(1 - \gamma)}$$

Table 10.2 Physical properties of Chromel and Alumel

Material	Absolute Q-values	Magnetic property	Composition
Alumel	- 18.3	Magnetic	90 % Ni, 10 % Cr
Chromel	+ 21.6	Non-magnetic	98 % Ni, 2 % Al

$$Q = -\frac{18.3 - 21.6\gamma}{-(\gamma - 1)}$$

$$Q = \frac{18.3 + 21.6\gamma}{(\gamma - 1)} \qquad (10.3)$$

The resistance of the sample was determined by passing a current through the leads C_1C_2 and measuring the potentials across leads A_1A_2. Similar to resistance measurements mentioned above, here also the pressure was calibrated using the bismuth transitions.

10.3 RESULTS

10.3.1 Variation of resistance with temperature :

The resistance of different specimens of WS_2 at different temperatures was measured by the two probe method already described in Chapter 2. Figures 10.5 and 10.6 show the variation of resistance with temperature for WS_2 crystals grown by DVT and CVT techniques respectively. The three curves marked as a, b and c in Fig. 10.5 and a', b', c' in Fig. 10.6 refer to specimens with absolutely plane faces, specimens having growth layers and specimens having spirals on their faces respectively.

The values of activation energy for DVT and CVT

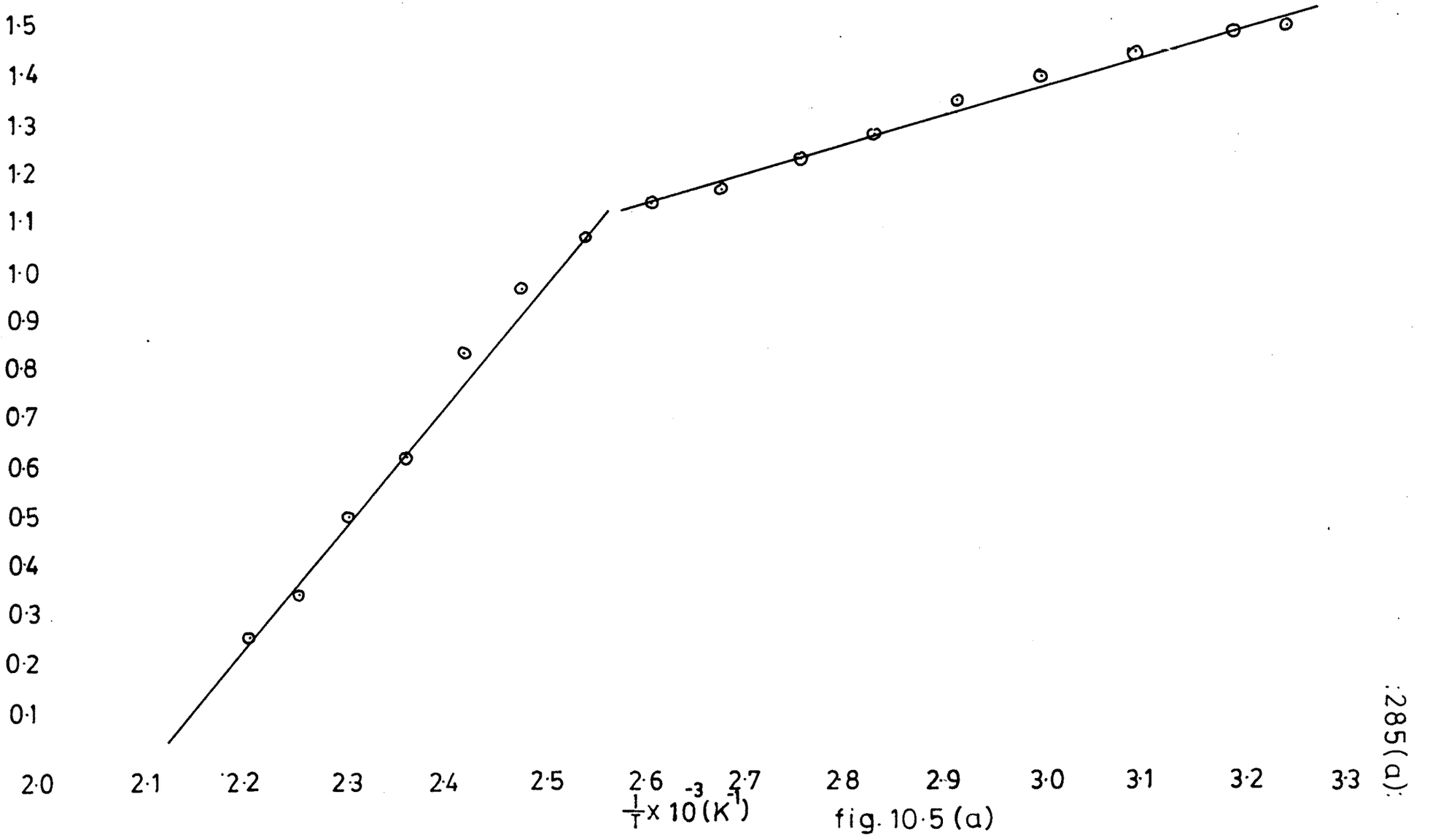
1·5
1·4
1·3
1·2
1·1
1·0
0·9
0·8
0·7
0·6
0·5
0·4
0·3
0·2
0·1
2·0
2·1
2·2
2·3
2·4
2·5
2·6
2·7
2·8
2·9
3·0
3·1
3·2
3·3
$\frac{1}{T} \times 10^{-3} (K^{-1})$

fig. 10·5 (a)

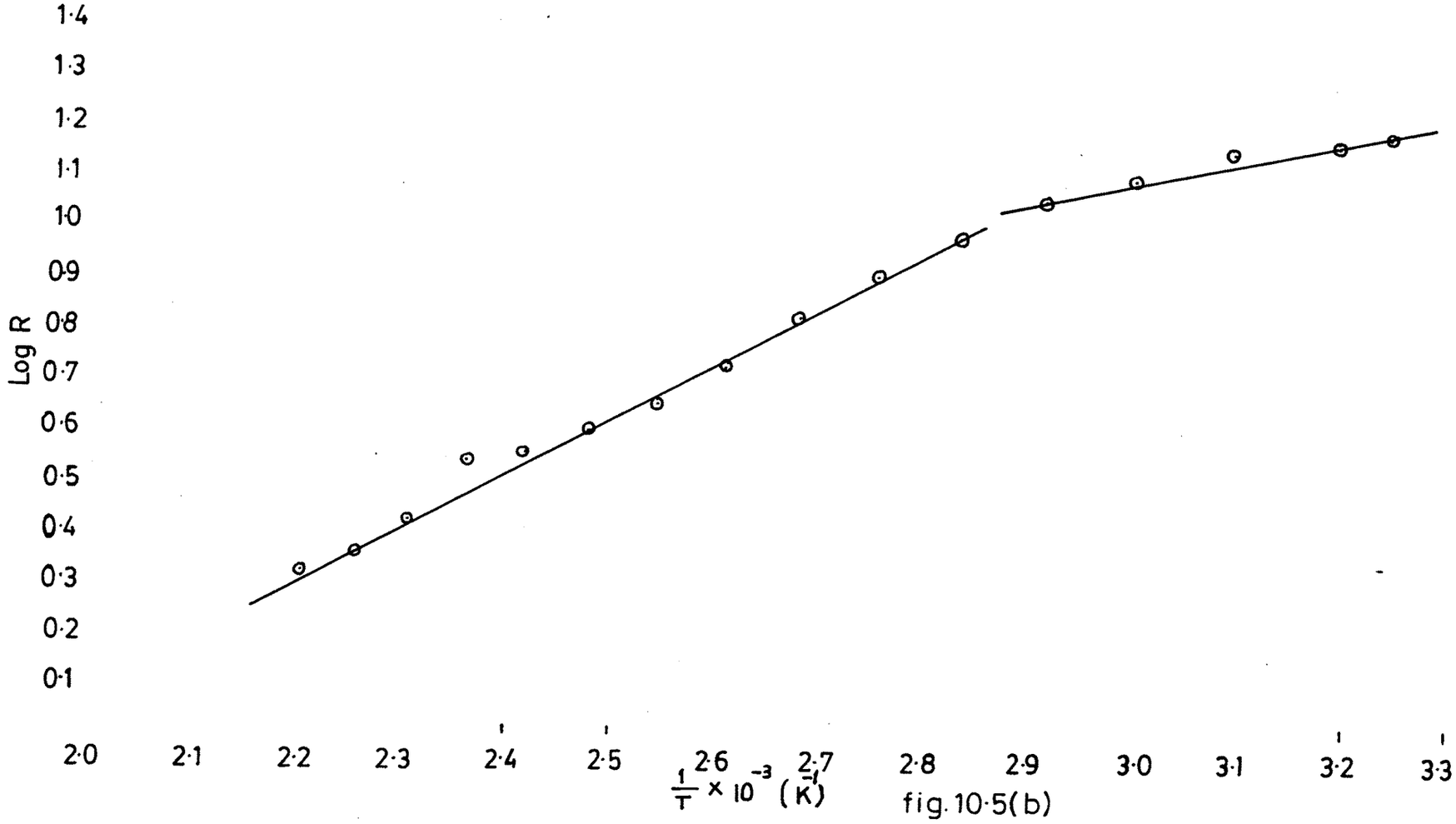

fig. 10·5(b)

:285 (b):

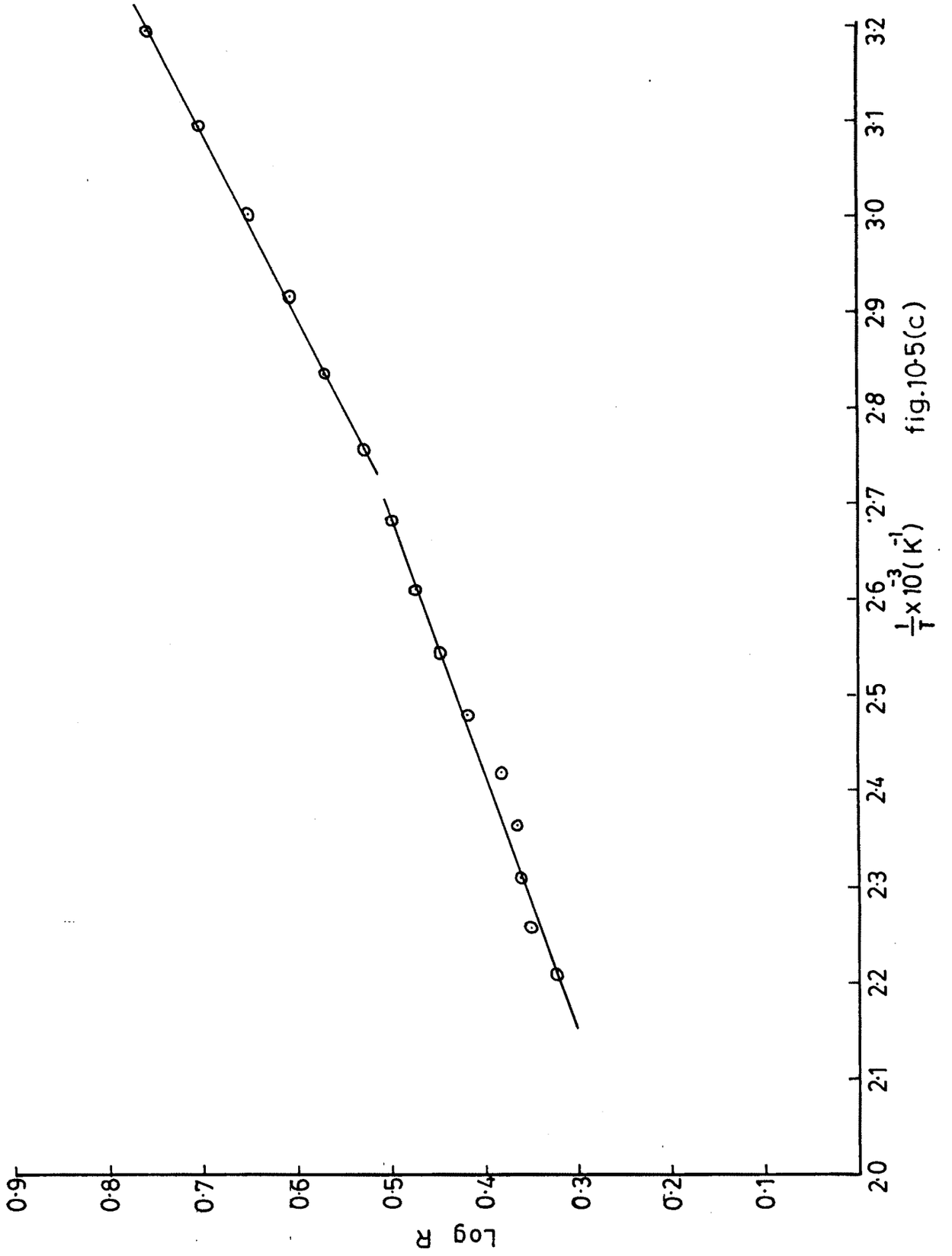
Log R
0·9
0·8
0·7
0·6
0·5
0·4
0·3
0·2
0·1
2·0
2·1
2·2
2·3
2·4
2·5
2·6
2·7
2·8
2·9
3·0
3·1
3·2
$\frac{1}{T} \times 10^{-3} (K^{-1})$

fig.10·5(c)

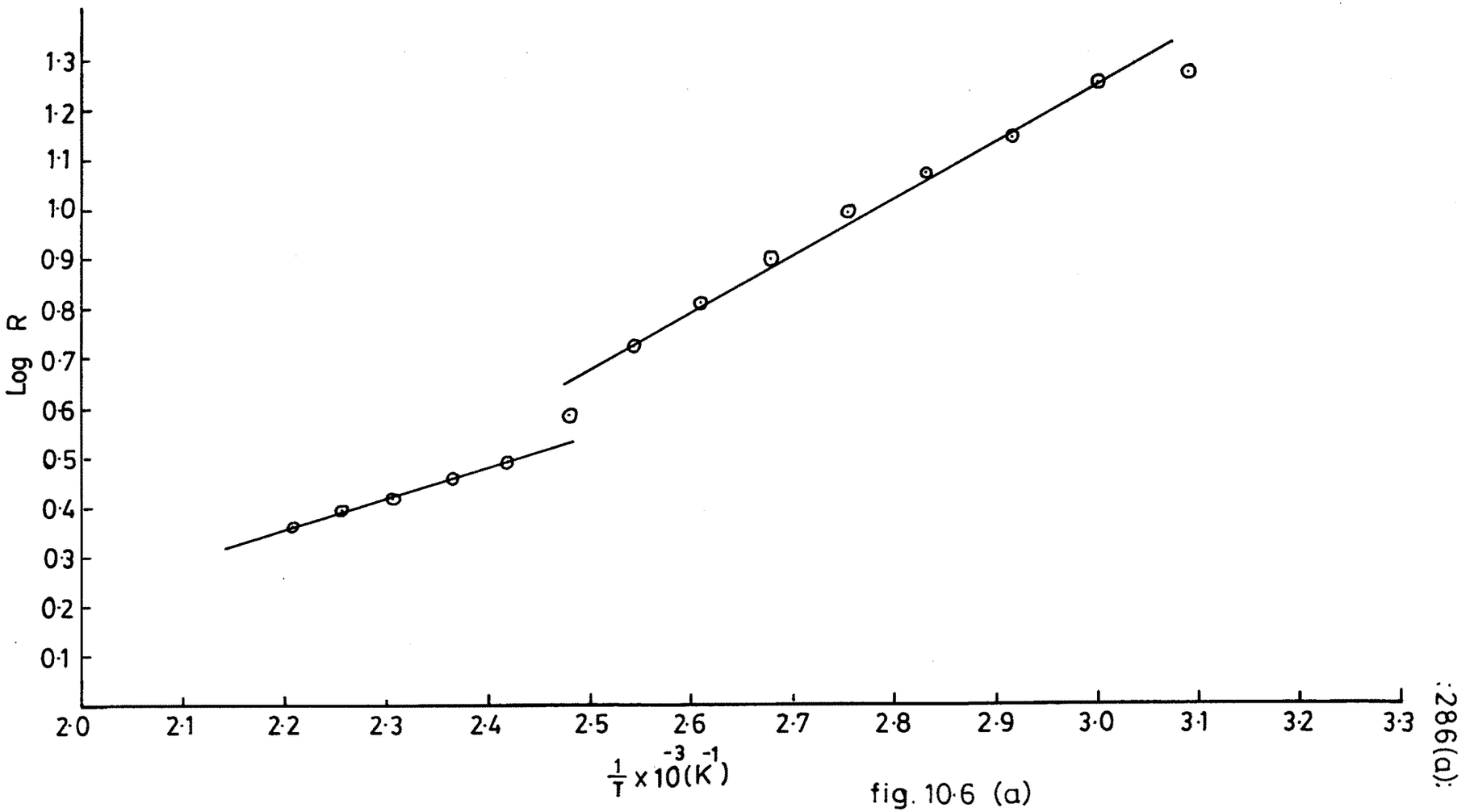

fig. 10·6 (a)

:286(a):

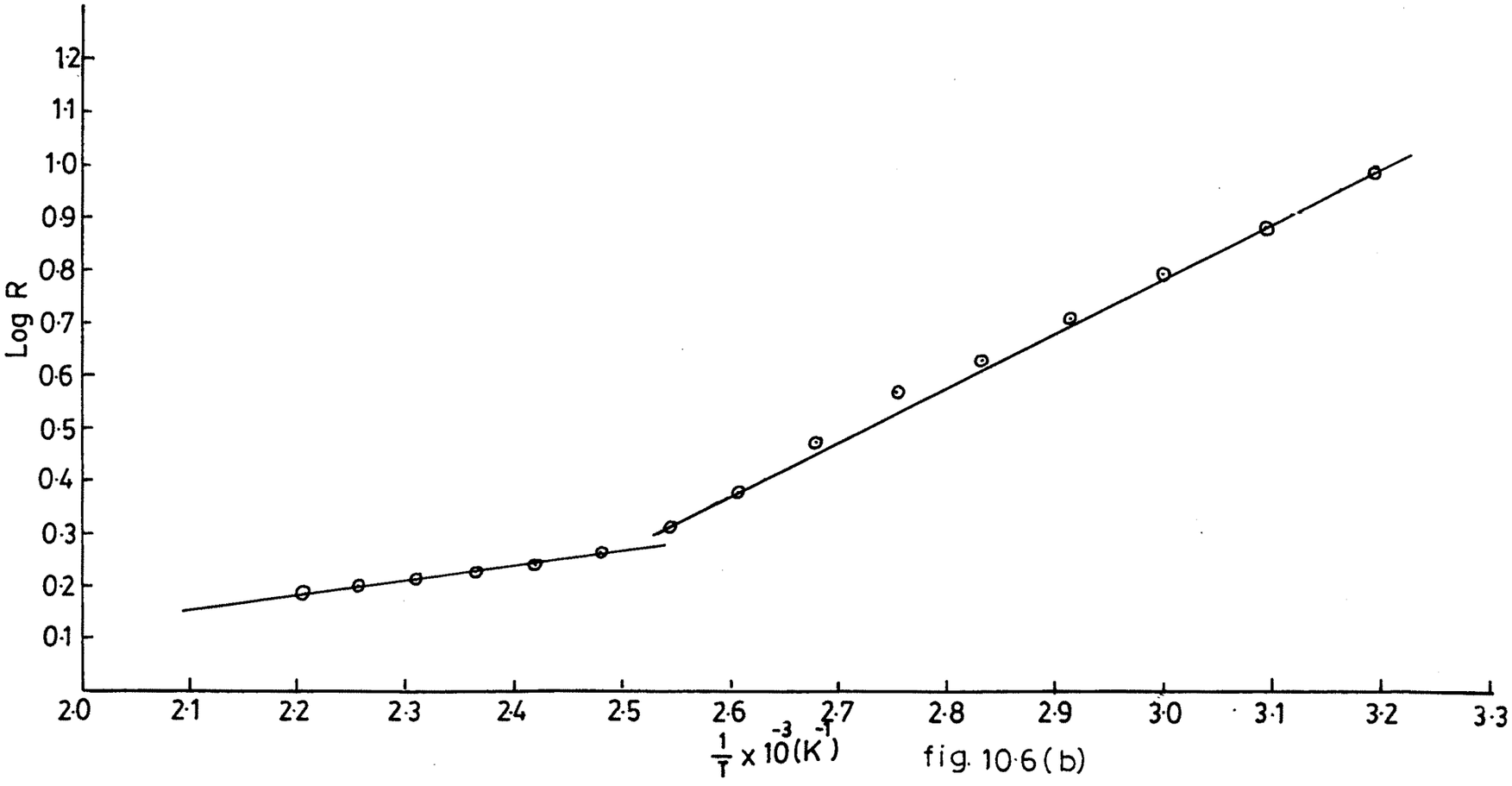
Log R
1·2
1·1
1·0
0·9
0·8
0·7
0·6
0·5
0·4
0·3
0·2
0·1
2·0
2·1
2·2
2·3
2·4
2·5
2·6
2·7
2·8
2·9
3·0
3·1
3·2
3·3
$\frac{1}{T} \times 10^{-3}(K^{-1})$

fig. 10·6 (b)

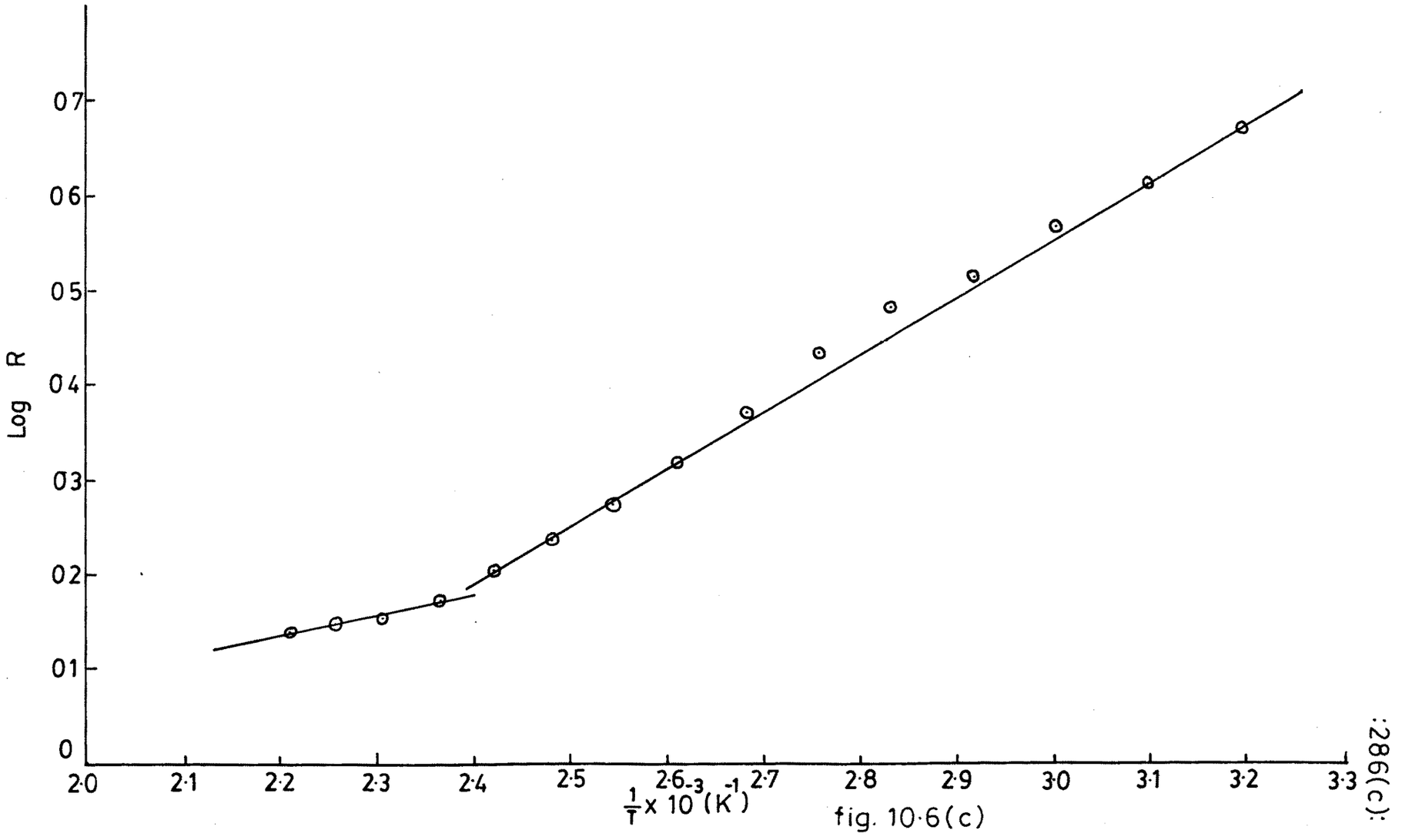

fig. 10·6(c)

:286(c):

grown WS_2 single crystals are mentioned in Table 10.3.

10.3.2 Variation of resistance with pressure

Figures 10.7 and 10.8 show the variation of resistance with pressure for DVT and CVT grown samples of WS_2 respectively. Captions to the figures indicate the nature of the specimen for which the variation has been depicted. A careful study of both these figures reveals the following points :

1. In both the cases of DVT and CVT grown samples, crystals having plane faces are more resistive as compared to those showing layered growth and spirals.

2. In all cases, the resistance of the CVT grown samples is less as compared to those grown by DVT.

3. The crystals showing layered growth are more resistive than those showing spirals

4. In each case, the resistance decreases monotonically with increase in pressure.

The variation of resistance with temperature clearly indicates that all the samples of WS_2 used in the present investigation are semiconductors. The Hall effect and thermoelectric power measurements further suggest that

Table 10.3 The values of activation energy for DVT and CVT grown WS_2 single crystals

Growth Process	Activation energy, E_a (eV)			
	Region I E_a (eV)	Temperature range K	Region II E_a (eV)	Temperature range K
DVT				
with absolutely plane faces	0.12	308-383	0.5	393-453
with growth layers	0.08	308-343	0.22	353-453
with spirals	0.10	308-363	0.07	373-453
CVT				
with absolutely plane faces	0.23	308-403	0.13	413-453
with growth layers	0.20	308-393	0.06	403-453
with spirals	0.12	308-413	0.04	423-453

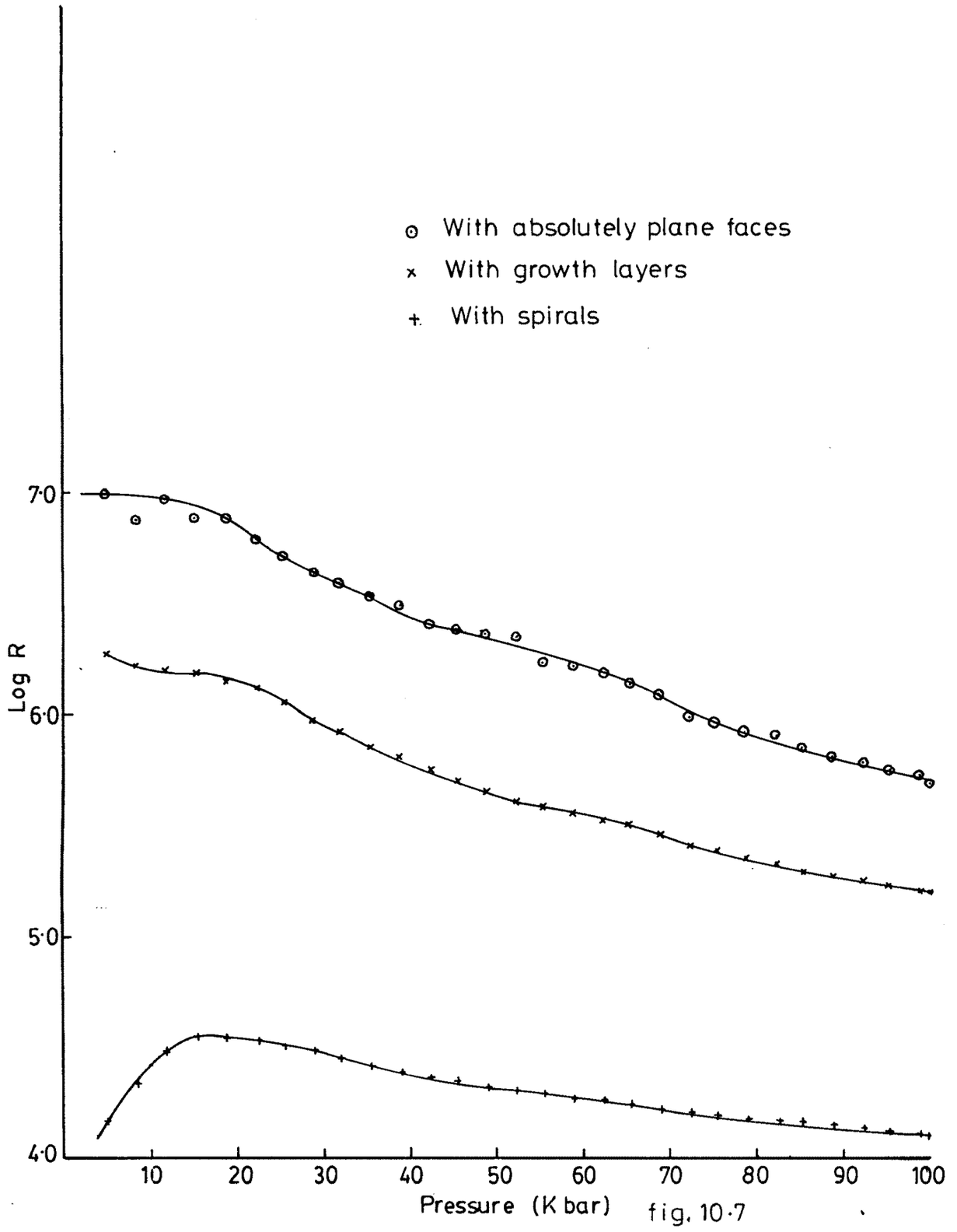
⊙ With absolutely plane faces
× With growth layers
+ With spirals
Log R
7·0
6·0
5·0
4·0
10
20
30
40
50
60
70
80
90
100
Pressure (K bar)

fig. 10·7

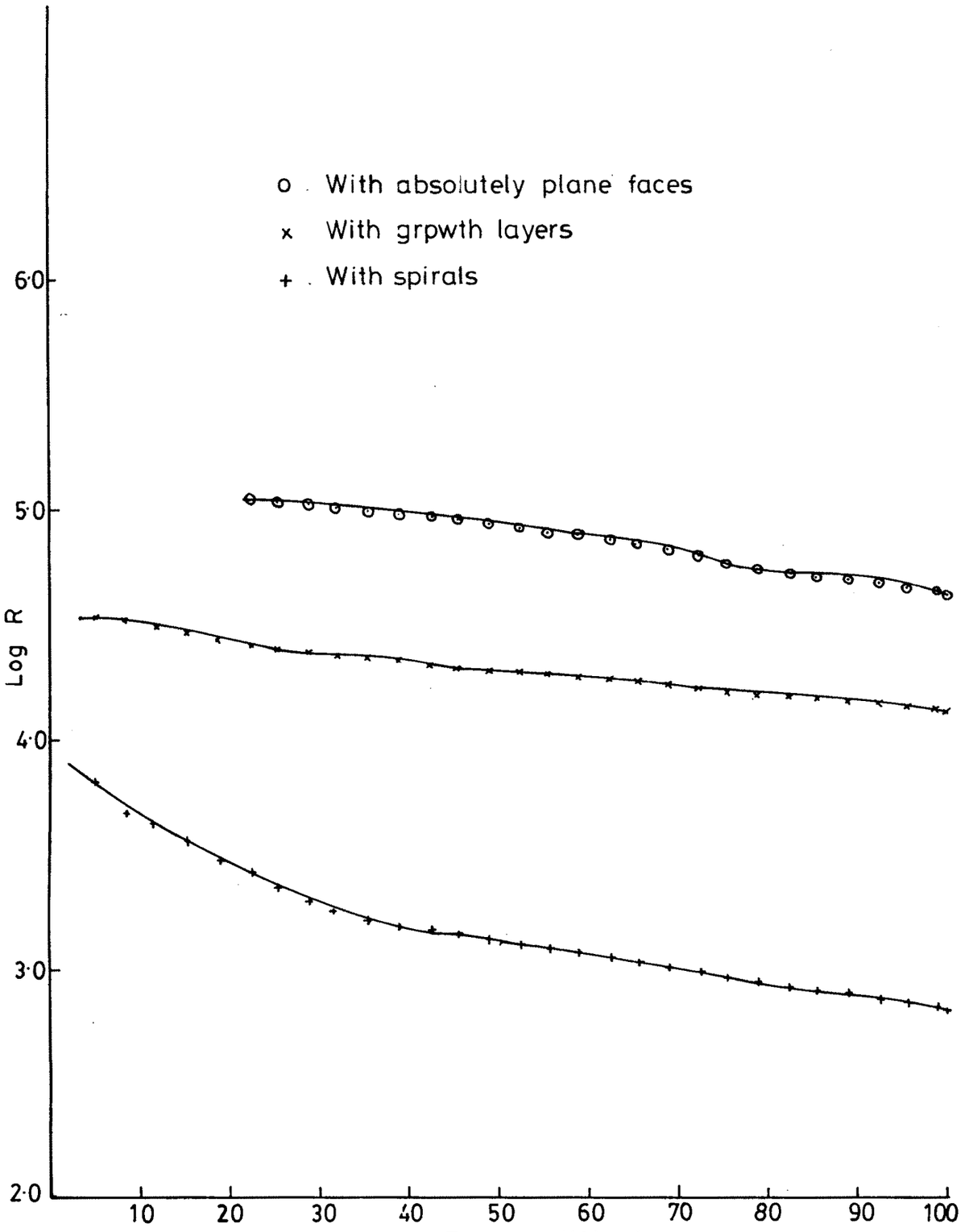
o With absolutely plane faces
x With grpwth layers
+ With spirals
6·0
5·0
4·0
3·0
2·0
Log R
10
20
30
40
50
60
70
80
90
100
Pressure (K bar)

fig.10·8

all of them are p-type extrinsic semiconductors. The extrinsic nature of the specimens is also supported by the activation energy values given in Table 10.3. In the extrinsic region, crystal imperfections may contribute to the number of carriers [7]. Due to this increase in carriers, the resistivity of crystals having imperfections would be low as compared to those which are having less imperfections. That this is true is clearly seen in the resistivity values of the different samples at the starting pressure.

Further, as seen in Fig. 10.9 the upper region of valence band in WS_2 is basically made up by the transition metal d_z2 states and d_{xy} and $d_{x^2-y^2}$ states form the conduction band. These bands are separated by nearly 1.78 eV. When pressure increases on WS_2 the separation of bands decreases and gives rise to a monotonic decrease of resistance with pressure as shown in Figs. 10.7 and 10.8.

With increase of pressure there is also a likelihood of increase in the number of imperfections. In this case the number of carriers would derive both from the decreased energy gap and from increase in the number of sources. This increase in the number of imperfections would also lower the mobility at all pressures. Thus in all cases

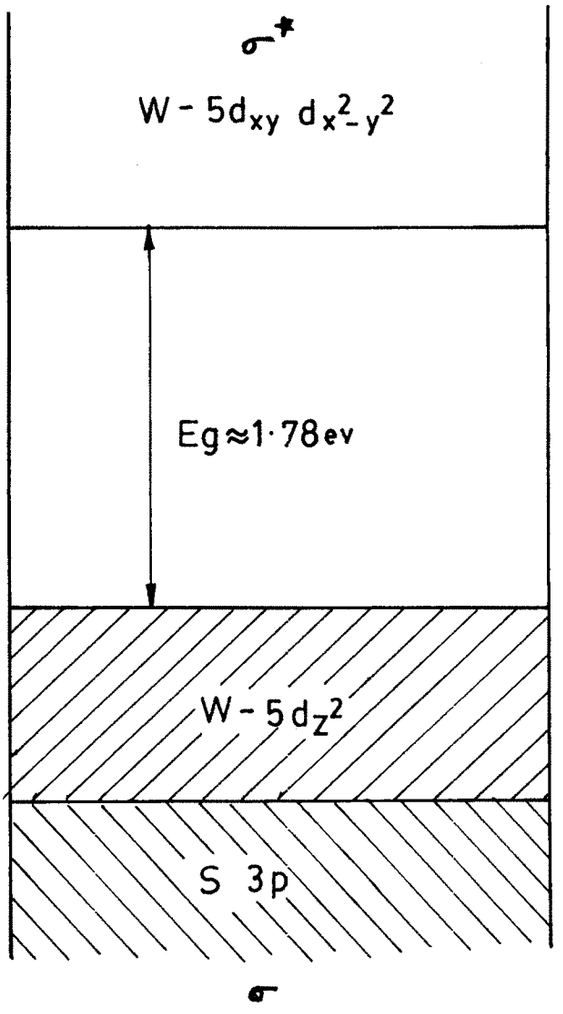

Band structure of WS_2

fig. 10·9

at lower pressures a high resistivity would be obtained. The observations described above clearly support this view.

10.3.3 Simultaneous variation of resistance and thermoelectric power with pressure :

For simultaneous measurement of thermoelectric power and resistances at different pressures, author has deliberately chosen all crystals grown by CVT method and having spirals upon their faces since they are having low room temperature resistivity as compared to others. Further it has been seen (Chapter 8) that though most of the CVT grown crystals are p-type, a few of them possess a n-type character.

The thermoelectric power and resistance variation with pressure for specimens which are representative of all such specimens having p-type and n-type character are respectively shown in Figs. 10.10 and 10.11. It may be mentioned that p-type and n-type nature of the specimens was also confirmed from the hot-probe technique.

In the case of p-type WS_2 (Fig. 10.10) with an initial increase from a value of 384 μV/K to 460 μV/K, TEP remains nearly constant upto the pressure of 30 Kbar and

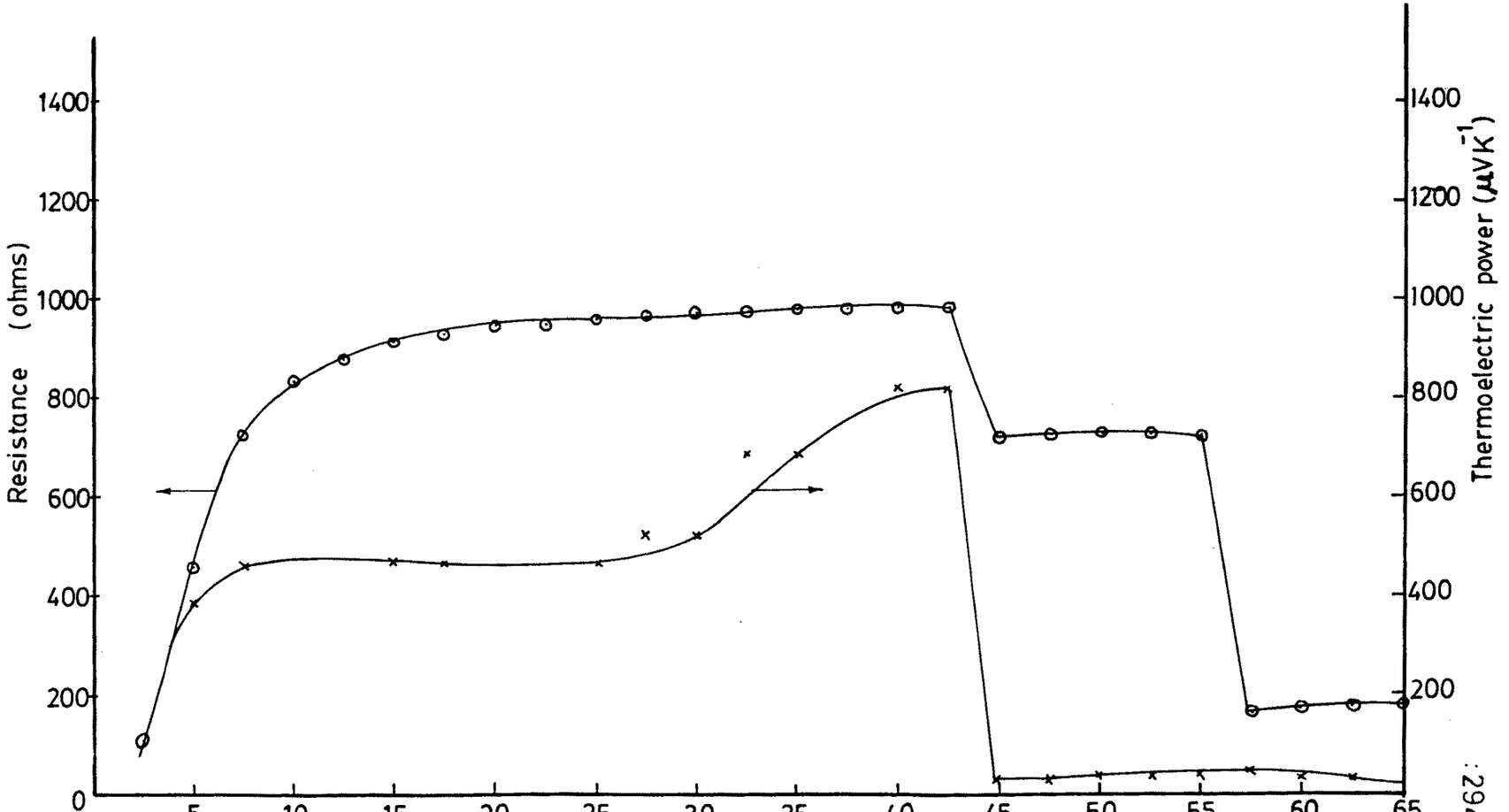
Resistance (ohms)
Thermoelectric power (μVK^{-1})
Pressure (K bar)
0
200
400
600
800
1000
1200
1400
5
10
15
20
25
30
35
40
45
50
55
60
65

fig. 10·10

thereafter steadily increases with pressure to a maximum value of 819.6 μV/K at 42.5 Kbar and abruptly decreases to a very low value of 26.946 μV/K. When the pressure is increased to 45 Kbar it is seen that with a further increase in pressure, TEP remains virtually independent of pressure.

The transition occuring at 42.5 Kbar is also very clearly seen in the variation of resistance with pressure. It is seen that resistance first of all increases steadily upto 12.5 Kbar and thereafter remains fairly constant up to 42.5 Kbar at which a sudden drop is seen in the value of resistance. The variation of resistance with pressure further points out a transition at 55 Kbar. No change in TEP is however observed in the region of 55 Kbar where the second transition is indicated by the variation of resistance.

In the case of n-type WS_2 (Fig. 10.11), the thermoelectric power has a negative value thus confirming the n-type character of the specimen. It is seen that the absolute value of thermoelectric power increases steadily with increase in pressure and reaches a maximum to 40 Kbar. Similar to p-type WS_2 (Fig. 10.10) here also one notices a sharp drop in thermoelectric power to a very low value which remains practically constant with a further increase in the pressure.

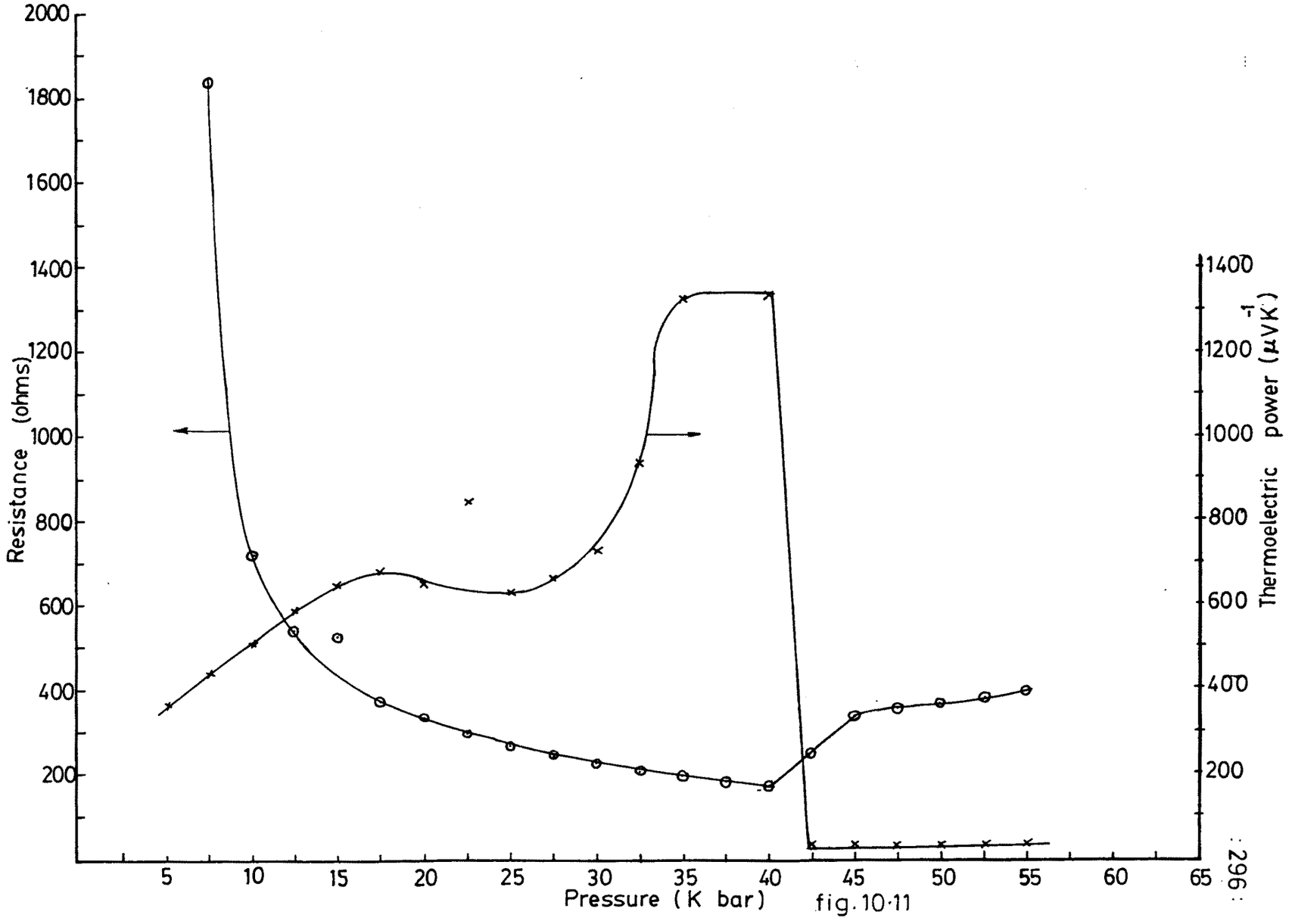
Resistance (ohms)
2000
1800
1600
1400
1200
1000
800
600
400
200
Thermoelectric power (μVK⁻¹)
1400
1200
1000
800
600
400
200
5
10
15
20
25
30
35
40
45
50
55
60
65
Pressure (K bar)
296 K

fig. 10·11

This transition at 40 Kbar is also very clearly pointed out from the variation of resistance with pressure. We observe that resistance monotonically decreases with increase in pressure upto 40 Kbar. An increase in pressure at 40 Kbar leads to a sudden increase in resistance.

Thus, we see that observation of Figs. 10.10 and 10.11 clearly indicate the presence of a phase transition in WS_2 in the region of 40-42.5 Kbar.

It can be noticed that there is an anomaly in the variation of resistance with pressure in the neighbourhood of the phase transition point. In the case of p-type WS_2 there is an increase in the resistance with pressure before the phase transition while in the case of n-type there is a decrease with pressure. With the data available at our disposal it is not possible to provide an explanation for this anomalous behaviour. The exact explanation might involve some more experimental work which can be taken up in future.

10.4 CONCLUSIONS

The measurements of resistance at different temperatures on WS_2 crystals (grown with and without a transporting agent and having different microstructures on their surfaces) have shown that all of them are

semiconductors. The Hall effect and thermoelectric power measurement (Chapter 8) have confirmed that they are p-type extrinsic semiconductors. The extrinsic nature of the crystals has also received further confirmation from the activation energy values obtained in different temperature ranges. The CVT grown crystals with spirals on the as grown faces have been found to be least resistive as compared to specimens with absolutely plane faces and having growth layers on their surfaces. In all cases the resistance was found to decrease monotonically with pressure. This has been attributed to the decrease in energy gap and increase in imperfections.

In the simultaneous measurement of thermo electrical power and resistance against pressure a transition was observed at 42.5 Kbar. The anomaly in resistance variation about the phase transition point could not be explained at this stage.

REFERENCES

[1] F. J. Clauss,
Solid Lubricants and Self-Lubricating Solids,
Academic Press (New York and London), (1972) 114.

[2] P. W. Bridgman,
Proc. Amer. Acad. Arts Sci., **81** (1952) 167.

[3] S. Minomura and H. G. Drickamer,
J. Appl. Phys., **34** (1963) 3043.

[4] G. A. N. Connell, J. A. Wilson and A. D. Yoffe,
J. Phys. Chem. Solids, **30** (1969) 287.

[5] A. J. Grant, J. A. Wilson and A. D. Yoffe,
Phil. Mag., **25** (1972) 625.

[6] H. D. Flack,
J. Appl. Crystallography, **5** (1972) 137.

[7] A. W. Webb, J. L. Feldman, E. F. Skelton and
L. C. Towle,
J. Phys. Chem. Solids, **37** (1976) 329.

[8] V. Vijaykumar, B. K. Godwal and S. K. Sikka,
Phys. Rev. B, **32** (1985) 4212.

[9] G. C. Kennedy and P. N. LaMori,
J. Geophys. Res., **67** (1962) 851.

[10] J. F. Cannon,
J. Phys. Chem. Ref. Data, 3 (1974) 78.

[11] A. K. Singh and G. Ramani,
Rev. Sci. Instrum., **49** (1978) 1324.

[12] Vijaykumar Viswanathan, S. N. Vaidya, Echur V. Sampath-Kumaran and Laxmi C. Gupta,
High-Temp. - High Press., **12** (1980) 649.

CAPTIONS TO THE FIGURES

Fig. 10.1 A resistivity cell for the opposed anvil set-up.

Fig. 10.2 Variation of the resistance of zone-refined 99.999 % pure bismuth with pressure.

Fig. 10.3 High pressure cell for the measurement of thermoelectric power using tungsten carbide opposed anvil set-up.

Fig. 10.4 Sample assembly for thermoelectric power and resistivity measurements.

Fig. 10.5 Variation of resistance with temperature in WS_2 single crystals grown by Direct Vapour Transport technique.

(a) with absolutely plane faces

(b) with growth layers

(c) with spirals.

Fig. 10.6 Variation of resistance with temperature in WS_2 single crystals grown by Chemical Vapour Transport technique.

(a) with absolutely plane faces

(b) with growth layers

(c) with spirals